



# Synthesis of synergetic phosphorus and cyano groups ( $-C\equiv N$ ) modified $g-C_3N_4$ for enhanced photocatalytic $H_2$ production and $CO_2$ reduction under visible light irradiation



Xiaolei Liu<sup>a</sup>, Peng Wang<sup>a,\*</sup>, Huishan Zhai<sup>a</sup>, Qianqian Zhang<sup>a</sup>, Baibiao Huang<sup>a,\*</sup>, Zeyan Wang<sup>a</sup>, Yuanyuan Liu<sup>a</sup>, Ying Dai<sup>b</sup>, Xiaoyan Qin<sup>a</sup>, Xiaoyang Zhang<sup>a</sup>

<sup>a</sup> State Key Lab of Crystal Materials, Shandong University, Jinan 250100, China

<sup>b</sup> School of Physics, Shandong University, Jinan, 250100, China

## ARTICLE INFO

### Keywords:

Synergetic  
 $g-C_3N_4$   
Photocatalytic  $H_2$  Production  
 $CO_2$  Reduction

## ABSTRACT

Graphitic carbon nitride ( $g-C_3N_4$ ) has become an attractive photocatalyst for solar energy conversion owing to its numerous advantages. Due to insufficient solar-light absorption and fast photogenerated carriers recombination, the photocatalytic activity of traditional  $g-C_3N_4$  material is unsatisfactory. In this work, P element and cyano groups ( $-C\equiv N$ ) incorporated into the  $g-C_3N_4$  framework is successfully fabricated by heat treatment of the mixed  $g-C_3N_4$  and  $NaH_2PO_2$ . The cyano groups ( $-C\equiv N$ ) originated from the de-protonation of  $-C-NH_2$  can enhance the light absorption and act as strong electron-withdrawing groups, which can promote the efficient separation of photo-generated electron-hole pairs. The P element doping can enhance the visible light absorption, shorten the band gap and suppress the recombination of photo-induced carriers. The synergistic effect of  $-C\equiv N$  functional groups and P element doping results in a 6.7 times enhanced photocatalytic  $H_2$  production activity and 1.58 times enhanced photocatalytic  $CO_2$  reduction activity than that of pristine  $g-C_3N_4$ . Experimental analysis indicates that the enhanced photocatalytic performance is mainly attributed to the enhanced light absorption and charge separation. Our work provides a new thought to design other high performance and low-cost  $g-C_3N_4$ -based photocatalytic materials for solar energy conversion.

## 1. Introduction

The excessive consumption of fossil fuels continues to deepen the worldwide energy crisis, accompanied by the release of a considerable amount of  $CO_2$ , which results in green-house effect and environmental pollution [1,2]. Photocatalytic  $H_2$  production from water and photocatalytic conversion  $CO_2$  to CO or hydrocarbon fuels are very promising ways to convert solar energy into other types of clean chemical fuels and reduce green-house effect [3,4]. Therefore, development and design of high efficient, low-cost and eco-friendly photocatalysts have become the main research hotspots in photocatalytic fields. Recent years, graphitic carbon nitride ( $g-C_3N_4$ ) as a polymeric-type semiconductor has received tremendous attention in photocatalytic fields owing to its low cost, peculiar thermal and chemical stability, non-toxicity and suitable band structure [5,6]. Therefore,  $g-C_3N_4$  has been recognized as a promising photocatalyst for solar energy conversion, such as photocatalytic  $H_2$  production and  $CO_2$  reduction [7–11].

$g-C_3N_4$  with band gap energy of 2.7 eV can be easily synthesized by

thermal polymerization melamine, dicyanamide, urea or thiourea. The conduction band bottom of  $g-C_3N_4$  is located at about -1.1 eV (vs. NHE), which is negative sufficiently for photocatalytic  $H_2$  production and  $CO_2$  reduction [12]. Although  $g-C_3N_4$  has so many advantages, its photocatalytic activity is still low due to the limited visible light absorption, small specific surface area and high recombination rate of photo-generated carriers. Thus, extensive strategies have been developed to improve the photocatalytic behavior of  $g-C_3N_4$ , such as nanostructure engineering [13–18], doping with heteroatoms to extend light absorption range and promote the separation efficiency of photo-generated electron-hole pairs [19–21], being exfoliated to a few layers [22,23], heterostructure construction [24–26] or being decorated with co-catalyst [27–32]. Particularly, the introduction of defects or doping with heteroatoms into the  $g-C_3N_4$  framework has been found to be effective ways to improve the photocatalytic activity [19,33–35]. Doping with heteroatoms or introducing defects in the tri-s-triazine repeating units of  $g-C_3N_4$  can modify the electronic structure and band gap, also act as reactive sites for photocatalytic reaction. In view of these advantages,

\* Corresponding authors.

E-mail addresses: [pengwangicm@sdu.edu.cn](mailto:pengwangicm@sdu.edu.cn) (P. Wang), [bbhuang@sdu.edu.cn](mailto:bbhuang@sdu.edu.cn) (B. Huang).

introducing defects and heteroatoms together in g-C<sub>3</sub>N<sub>4</sub> may bring better performance than alone. But the current researches in g-C<sub>3</sub>N<sub>4</sub> are always focusing on introducing defects or heteroatoms alone, and as for defects studies, a relatively high reaction temperature and reducing atmosphere (like H<sub>2</sub> and NH<sub>3</sub>) are both necessary to realize the incorporation of defect into g-C<sub>3</sub>N<sub>4</sub> structure [36,37]. Therefore, simple and effective methods are required toward the synthesis of both defects and heteroatoms modified g-C<sub>3</sub>N<sub>4</sub>.

In this research, we present a simple and effective method to synthesize both defect and heteroatoms modified g-C<sub>3</sub>N<sub>4</sub> through second calcination of the mixed g-C<sub>3</sub>N<sub>4</sub> and NaH<sub>2</sub>PO<sub>2</sub> under inert atmosphere. During calcination, NaH<sub>2</sub>PO<sub>2</sub> decomposes to gaseous PH<sub>3</sub> and solid-state Na<sub>2</sub>HPO<sub>4</sub> at temperature greater than 150 °C according to the reaction: 2NaH<sub>2</sub>PO<sub>2</sub>(s)  $\xrightarrow{\Delta}$  PH<sub>3</sub>(g) + Na<sub>2</sub>HPO<sub>4</sub>(s) [38]. Solid-state Na<sub>2</sub>HPO<sub>4</sub> can react with g-C<sub>3</sub>N<sub>4</sub> to produce cyano terminal C≡N groups, and gaseous PH<sub>3</sub> can dope P element into g-C<sub>3</sub>N<sub>4</sub> structure. The formation of –C≡N functional groups can not only enhance the light absorption but also act as strong electron-withdrawing groups in g-C<sub>3</sub>N<sub>4</sub> to promote the efficient separation of photogenerated carriers [33,42], the doping of P heteroatom into g-C<sub>3</sub>N<sub>4</sub> structure can extend the light absorption, increase the electric conductivity and suppress the recombination of photo-generated electron-hole pairs [39]. The synergistic effect of –C≡N functional groups and doping of P heteroatom results in a 6.7 times enhanced photocatalytic H<sub>2</sub> production activity and 1.58 times enhanced photocatalytic CO<sub>2</sub> reduction activity than that of pristine g-C<sub>3</sub>N<sub>4</sub>. This work provides a simple and effective route to realize both defects and heteroatoms modified g-C<sub>3</sub>N<sub>4</sub>, the enhanced light absorption and efficient separation of photo-generated carriers are benefit for high efficient solar energy conversion.

## 2. Experimental section

### 2.1. Synthesis of pristine g-C<sub>3</sub>N<sub>4</sub>

Pristine g-C<sub>3</sub>N<sub>4</sub> was prepared by traditional thermal polycondensation. Briefly, 6 g of urea and 6 g of dicyandiamide were grounded in an agate mortar for 20 min. Then, the mixture was calcined at 550 °C in a muffle furnace for 4 h using a heating rate of 5 °C min<sup>-1</sup> in air. After cooling naturally, the yellow product was grounded for 30 min to obtain a powder sample. The obtained product was 4.8 g and the yield was 40%.

### 2.2. Preparation of phosphorus and cyano groups (–C≡N) modified g-C<sub>3</sub>N<sub>4</sub>

Briefly, the as-prepared g-C<sub>3</sub>N<sub>4</sub> (0.4 g) was mixed with NaH<sub>2</sub>PO<sub>2</sub> (0.2 g) at a weight ratio of 2:1, grounded in a mortar sufficiently, and then calcined in a tube furnace under Ar atmosphere at different temperatures (300 °C, 350 °C, 400 °C, 425 °C, 450 °C and 500 °C) for 60 min using a heating rate of 10 °C min<sup>-1</sup>. Residual PH<sub>3</sub> was very dangerous, so strong oxidizing sodium hypochlorite solution (1 mol/L) was used to absorb the residual PH<sub>3</sub> at the end of the vent. After cooling naturally, the resultant products were washed with water, NaOH (0.1 mol/L), HCl (0.1 mol/L) and water again to remove any unreacted and potentially detrimental surface species. The achieved products were denoted as g-C<sub>3</sub>N<sub>4</sub> -x, x indicated the heating temperature. By contrast, the preparation process of g-C<sub>3</sub>N<sub>4</sub> treated by Na<sub>2</sub>HPO<sub>4</sub> was the same as g-C<sub>3</sub>N<sub>4</sub> treated by NaH<sub>2</sub>PO<sub>2</sub> except replacing NaH<sub>2</sub>PO<sub>2</sub> by Na<sub>2</sub>HPO<sub>4</sub>.

### 2.3. Material characterization

X-ray diffraction patterns (XRD) were recorded on a Bruker AXS D8 diffractometer equipped with Cu K $\alpha$  radiation ( $\lambda = 0.154056$  nm). Diffuse reflectance UV-vis absorption spectroscopy was recorded using Shimadzu UV-2550 spectrophotometer, with BaSO<sub>4</sub> performing

as a reference. Morphologies and microstructures of the products were characterized by scanning electron microscopy (Hitachi S-4800) equipped with an Energy Dispersive Spectrometer (EDS) and transmission electron microscopy (JEOL JEM-2100F). X-ray photoelectron spectroscopy (XPS, Thermo Fisher Scientific Escalab 250 spectrometer) with monochromatized Al K $\alpha$  excitation was used to analyze quantitatively the chemical composition of the products and C 1 s (284.8 eV) was used to calibrate the peak positions. Fourier-transform infrared (FTIR) spectra were recorded using the FT-IR spectrometer (Nicolet Nexus 670). The PL measurement was analyzed on a Hitachi F-4500 fluorescence spectrophotometer at room temperature and obtained with excitation wavelength at 360 nm. The time resolved fluorescence spectra were recorded at 460 nm using a 377.8 nm excitation by Edinburgh FLS920 PL, decay curves were fitted by using a biexponential decay function to obtain deconvolution of the instrument response function. The Brunauer-Emmett-Teller (BET) specific surface area was measured by a Micromeritics ASAP 2020 apparatus. Isotopic experiment was performed using <sup>13</sup>CO<sub>2</sub> (purity: 99%), and the produced CO was analyzed by gas chromatography-mass spectrometry (GC-MS).

### 2.4. Photoelectrochemical measurement

Photocurrent response and electrochemical impedance spectroscopy (EIS) measurements were measured by a Princeton Applied Research EG&G 263 A electrochemical analyzer using a standard three-electrode mode with 0.2 M Na<sub>2</sub>SO<sub>4</sub> (pH = 6.8) solution as the electrolyte, the catalyst-coated FTO glass as the working electrode, a Pt sheet as the counter electrode and Ag/AgCl as the reference electrode. The light source was a 300 W Xe arc lamp coupled with an AM1.5 global filter. The photocurrent response was measured at 1.0 V. To prepare the working electrodes, 50 mg of the as-prepared samples were dispersed in absolute ethanol and grounded for 30 min, the suspension was spin-coated on cleaned fluorine doped tin oxide (FTO) glass and then calcined at 450 °C for 60 min in a muffle furnace.

### 2.5. Photocatalytic test

Photocatalytic hydrogen production was performed in a Pyrex top-irradiation reaction vessel connected to a glass closed gas circulation system and kept at 15 °C during reaction. 100 mg of catalyst powder was well dispersed in a 100 mL mixed solution containing triethanolamine (10 vol.%) as a sacrificial agent. 1 wt% Pt was photo-deposited on the catalysts through photo-reduction of H<sub>2</sub>PtCl<sub>6</sub> dissolved in the reactant solution. The system was evacuated several times to remove air completely and then irradiated by a 300 W Xe lamp equipped with a 420 nm cut-off filter ( $\lambda \geq 420$  nm) as the light source. The distance between the light source and the solution was about 14 cm, and the average power energy density of the irradiation was about 200 mW/cm<sup>2</sup> measured by PL-MW2000 spectroradiometer (PerfectLight, China). The gas production in the reaction system was sampled and measured with a gas chromatograph (GC-7806, Shiweipx). In order to investigate the stability of the product, cycling experiment was taken out. The detailed procedures were as follows: after irradiation for 3 h, the produced H<sub>2</sub> was removed by a vacuum pump. Then, the next cycle began under the same condition. And the action spectra were measured under the same conditions with band-pass monochromatic filters centered at 420, 450, 520 and 600 nm, respectively. The quantum efficiency (QE) for H<sub>2</sub> production was measured with a 300 W Xe-lamp equipped with a 420 nm ( $\pm 10$  nm) monochromatic filter as the light source. The irradiation area was 4 cm<sup>2</sup> and the average energy density was 55 mW/cm<sup>2</sup>. The QE was calculated using the following equation:

$$QE = \frac{2 \times \text{the number of evolved hydrogen}}{\text{the number of incident photons}} \times 100\%$$

Photocatalytic CO<sub>2</sub> reduction was performed in a 250 mL Pyrex top-irradiation reactor at ambient temperature and atmospheric pressure.

The opening of the reactor was sealed with silicone rubber plug to form a closed system, and a 300 W Xe lamp equipped with a 420 nm cut-off filter ( $\lambda \geq 420$  nm) as the light source. Before reaction, 1 wt% Au was deposited on the catalysts through chemical reduction of HAuCl<sub>4</sub> using NaBH<sub>4</sub> as reductant. 100 mg of as-prepared product was well dispersed in a 100 mL solution containing 1 M NaHCO<sub>3</sub>, and the system was bubbled with high purity CO<sub>2</sub> for 10 min. And the contrast experiment was carried out without adding NaHCO<sub>3</sub> and bubbling high purity CO<sub>2</sub>, before irradiation, the system was vacuumed by pump and high purity Ar gas was bubbled for 30 min to ensure that almost no CO<sub>2</sub> took part in the reaction. The gas production in the reaction system was sampled and measured with a gas chromatograph (GC-7920, CEAULIGHT, Beijing) equipped with a flame ionized detector. In order to study the stabilities of the products, cycling experiment was taken out. The detailed procedures were as follows: after irradiation for 3 h, the produced CO was removed by blowing high purity CO<sub>2</sub>. Then, the next cycle began under the same condition. And the isotopic experiment was performed using <sup>13</sup>CO<sub>2</sub> (purity: 99%), and the produced CO was analyzed by gas chromatography-mass spectrometry (GC-MS).

### 3. Results and discussion

The phase structures of as-prepared products were identified by powder X-ray diffraction analysis. As shown in Fig. 1, the pristine g-C<sub>3</sub>N<sub>4</sub> exhibits two distinct characteristic peaks at 13.1° and 27.4°, respectively. The minor diffraction peak at 13.1° is corresponded to the (1 0 0) plane and ascribed to the in-plane structural packing motif of tri-stiazine [40]. The high-angle diffraction peak at 27.4° is the characteristic peak of an interlayer stacking of conjugated aromatic systems, which is indexed to the (0 0 2) plane for graphitic materials [41]. All of the XRD patterns of g-C<sub>3</sub>N<sub>4</sub> treated with NaH<sub>2</sub>PO<sub>2</sub> at different temperatures are very similar to that of pristine g-C<sub>3</sub>N<sub>4</sub>, indicating that the basic crystal structure of g-C<sub>3</sub>N<sub>4</sub> is preserved with NaH<sub>2</sub>PO<sub>2</sub> treatment. However, both the diffraction peaks at 13.1° and 27.4° are broadened and gradually weakened, suggesting that the ordered and periodic structures within the framework of g-C<sub>3</sub>N<sub>4</sub> are broken during the heat treatment with NaH<sub>2</sub>PO<sub>2</sub>.

The chemical structures of as-prepared products were analyzed by Fourier transform infrared (FTIR) spectra, as shown in Fig. 2. In Fig. 2a, the pristine g-C<sub>3</sub>N<sub>4</sub> shows a spectrum with typical characteristic peaks: the peak at 810 cm<sup>-1</sup> is the characteristic breathing mode of s-triazine ring system, the peaks located between 1000 and 1800 cm<sup>-1</sup> originate from the typical stretching vibration modes of C=N and C—N heterocycles, while multiple broad peaks in 3000–3500 cm<sup>-1</sup> region are

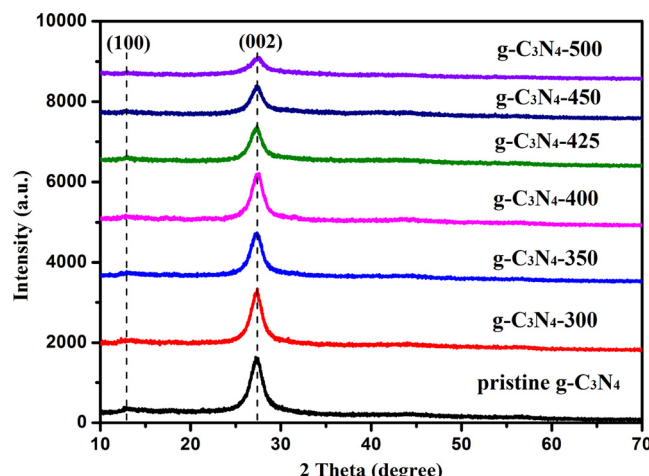


**Fig. 1.** XRD patterns of pristine g-C<sub>3</sub>N<sub>4</sub> and g-C<sub>3</sub>N<sub>4</sub> after heat treatment with NaH<sub>2</sub>PO<sub>2</sub> at different temperatures (300 °C, 350 °C, 400 °C, 425 °C, 450 °C and 500 °C).

ascribed to N—H stretching vibrations [22]. For the g-C<sub>3</sub>N<sub>4</sub> products after heat treatment with NaH<sub>2</sub>PO<sub>2</sub> at different temperatures, a new vibration band at 2180 cm<sup>-1</sup> appears, belonging to an asymmetric stretching vibration of cyano groups (—C≡N) [33,42,43]. The vibration peak intensity of cyano group increases and the peak intensity of N—H stretching vibrations decreases gradually with the heating temperature increasing, which may prove that the cyano groups originate from the de-protonation of —C—NH<sub>2</sub>. The intensity of the peak at 810 cm<sup>-1</sup> decreases gradually with the heating temperature increasing, suggesting that the s-triazine ring system is destroyed, which is consistent with the XRD result. During heating, NaH<sub>2</sub>PO<sub>2</sub> decomposes into gaseous PH<sub>3</sub> and solid-state Na<sub>2</sub>HPO<sub>4</sub>. In Fig. 2 b, the FTIR spectrum of g-C<sub>3</sub>N<sub>4</sub> after heat treatment at 425 °C alone in Ar atmosphere shows no difference with pristine g-C<sub>3</sub>N<sub>4</sub>. However, the cyano groups (—C≡N) appears in the FTIR spectra of g-C<sub>3</sub>N<sub>4</sub> after heat treatment with Na<sub>2</sub>HPO<sub>4</sub> at different temperatures, suggesting that the appearance of cyano groups may be caused by Na<sub>2</sub>HPO<sub>4</sub>.

Further detailed surface chemical status and chemical compositions of pristine g-C<sub>3</sub>N<sub>4</sub> and g-C<sub>3</sub>N<sub>4</sub> after heat treatment with NaH<sub>2</sub>PO<sub>2</sub> for 1 h at 425 °C were analyzed with X-ray photoelectron spectroscopy (XPS) measurements. As compared in Fig. 3a, XPS survey spectra of both pristine g-C<sub>3</sub>N<sub>4</sub> and g-C<sub>3</sub>N<sub>4</sub>-425 contain three sharp peaks at 288.2, 398.72 and 532 eV, which are respectively assigned to C 1s, N 1s, and O 1s signals. The O 1s signal may be from the absorbed H<sub>2</sub>O and CO<sub>2</sub> on the surface of the products. In order to find the difference between pristine g-C<sub>3</sub>N<sub>4</sub> and g-C<sub>3</sub>N<sub>4</sub>-425, the corresponding high resolution XPS spectra of C, N and P are shown in Fig. 3b-d. For the pristine g-C<sub>3</sub>N<sub>4</sub>, the high resolution C 1s spectrum is fitted into three peaks, the peak centered at 284.8 eV is assigned to carbon impurities, the main peak centered at 288.2 eV is ascribed to sp<sup>2</sup>-bonded carbon of N≡C—N in the aromatic ring and the peak centered at 286.27 eV is ascribed to the sp<sup>2</sup> C atoms in the aromatic ring attached to the —NH<sub>2</sub> group [5]. The high resolution N 1s spectrum is also fitted into three peaks, which are located at 398.72, 400.22, and 401.43 eV for sp<sup>2</sup>-hybridized nitrogen (N=C=N), tertiary nitrogen (N—(C)<sub>3</sub>), and terminal amino groups (C—NH), respectively [2]. As for g-C<sub>3</sub>N<sub>4</sub> after heat treatment with NaH<sub>2</sub>PO<sub>2</sub> for 1 h at 425 °C, a little difference is appeared relative to the pristine g-C<sub>3</sub>N<sub>4</sub> that the peak at 286.15 eV for the sp<sup>2</sup> C atoms in the aromatic ring attached to the —NH<sub>2</sub> group and the peak at 401.29 eV for terminal amino groups (C—NH) are a little deflected. Combining this tiny variation, we speculate that the cyano groups (—C≡N) originate from de-protonation of —C—NH<sub>2</sub> by oxidizing Na<sub>2</sub>HPO<sub>4</sub>. This result agrees well with the FTIR result. No P element is detected in the pristine g-C<sub>3</sub>N<sub>4</sub>, but in Fig. 3d, obvious P element is detected in the g-C<sub>3</sub>N<sub>4</sub>-425 product. The peak of P2p binding energy is centered at 133.9 eV, which is typical for the P—N bond (P—C bonding would be 1–2 eV lower) [39,40]. So the P element is doped into the g-C<sub>3</sub>N<sub>4</sub> system, the weight ratio of P provided by EDS result is about 0.18%, the detailed information can be seen in Section 4, supporting information (Table S1).

The optical absorption properties of the prepared products were studied by UV-vis diffuse reflection spectra. As shown in Fig. 4a, the pristine g-C<sub>3</sub>N<sub>4</sub> shows the typical absorption edge at about 450 nm and g-C<sub>3</sub>N<sub>4</sub> heating without NaH<sub>2</sub>PO<sub>2</sub> at 425 °C in Ar atmosphere shows only a little variation. However, when the g-C<sub>3</sub>N<sub>4</sub> is treated with NaH<sub>2</sub>PO<sub>2</sub> at different heating temperatures (300 °C, 350 °C, 400 °C, 425 °C, 450 °C and 500 °C) in Ar atmosphere, the gradual red-shift to longer wavelength is observed following the enhanced heating temperature. Consistent with the absorption results, the colour of the products suffers a corresponding change from yellow to brown as the treatment temperature increases (more detailed information can be seen in Fig. S2). The significant red-shift of the absorption wavelength indicates that the products can absorb more solar energy, which is benefit for the photocatalytic activity. And the enhanced light absorption may derive from the P element doping and the formation of cyano groups (—C≡N). The influence in the light absorption of cyano groups

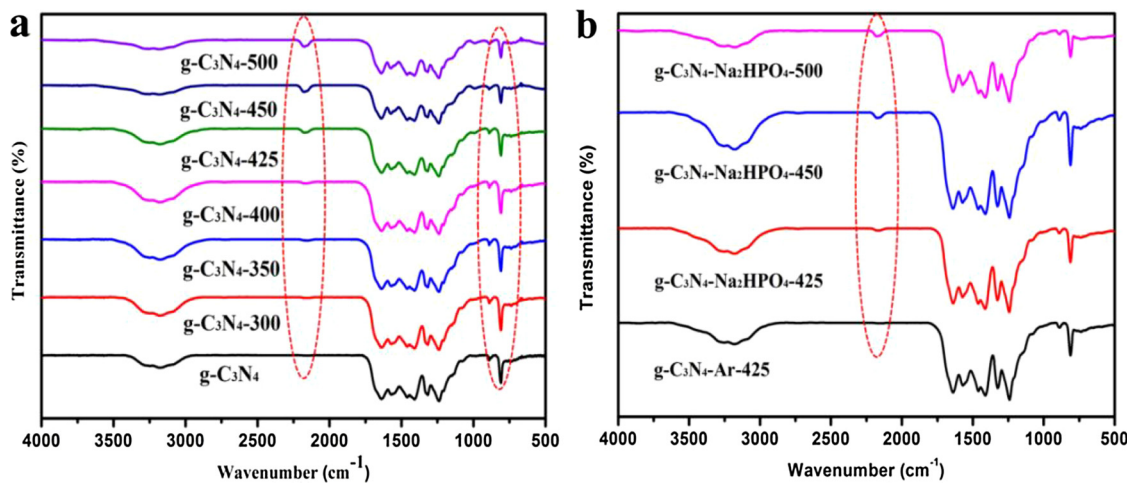


**Fig. 2.** (a) The FTIR spectra of pristine  $\text{g-C}_3\text{N}_4$  and  $\text{g-C}_3\text{N}_4$  after heat treatment with  $\text{NaH}_2\text{PO}_2$  for 1 h at different temperatures ( $300\text{ }^\circ\text{C}$ ,  $350\text{ }^\circ\text{C}$ ,  $400\text{ }^\circ\text{C}$ ,  $425\text{ }^\circ\text{C}$ ,  $450\text{ }^\circ\text{C}$  and  $500\text{ }^\circ\text{C}$ ), (b) The FTIR spectra of  $\text{g-C}_3\text{N}_4$  after heat treatment at  $425\text{ }^\circ\text{C}$  alone in Ar atmosphere and  $\text{g-C}_3\text{N}_4$  after heat treatment with  $\text{Na}_2\text{HPO}_4$  for 1 h at different temperatures ( $425\text{ }^\circ\text{C}$ ,  $450\text{ }^\circ\text{C}$  and  $500\text{ }^\circ\text{C}$ ).

( $-\text{C}\equiv\text{N}$ ) can be seen in Section 3 (Fig. S3), supporting information. Fig. 4 b shows the calculated band gaps for  $\text{g-C}_3\text{N}_4$  and  $\text{g-C}_3\text{N}_4\text{-X}$  (X means the temperature of heat treatment). The band gaps of the samples determined from the Kubelka–Munk transformation are reduced

from 2.60 ( $\text{g-C}_3\text{N}_4$ ), to 2.54 ( $\text{g-C}_3\text{N}_4\text{-300}$ ), to 2.46 ( $\text{g-C}_3\text{N}_4\text{-350}$ ), to 2.28 ( $\text{g-C}_3\text{N}_4\text{-400}$ ), to 2.22 ( $\text{g-C}_3\text{N}_4\text{-425}$ ), to 2.20 ( $\text{g-C}_3\text{N}_4\text{-450}$ ) to 2.18 eV ( $\text{g-C}_3\text{N}_4\text{-500}$ ).

The photocatalytic activities of as-prepared products were evaluated

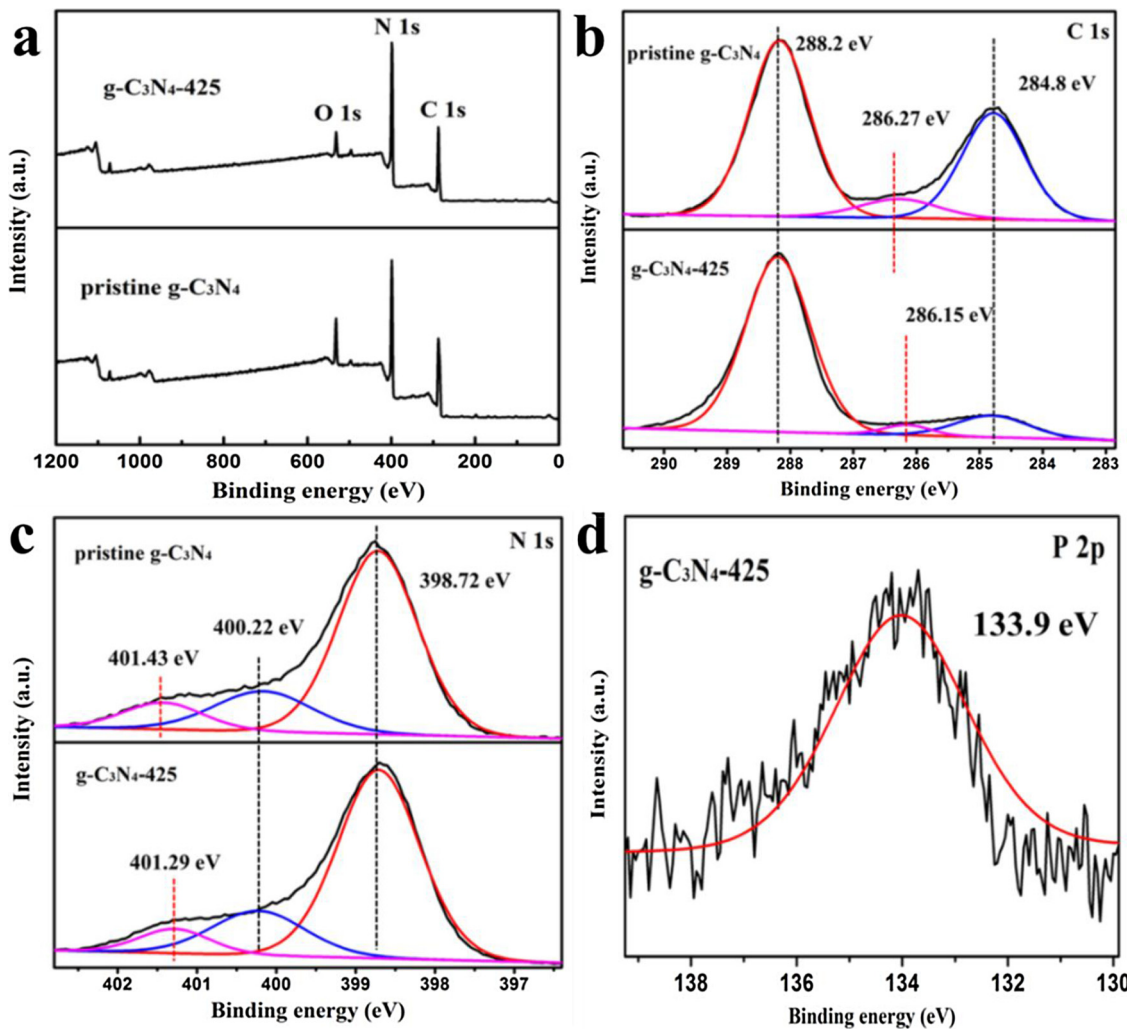


**Fig. 3.** (a) XPS survey spectra, (b–c) high-resolution XPS spectra of C 1 s region and N 1 s region for pristine  $\text{g-C}_3\text{N}_4$  and  $\text{g-C}_3\text{N}_4\text{-425}$ , respectively, (d) high-resolution XPS spectrum of P 2p for  $\text{g-C}_3\text{N}_4\text{-425}$ .

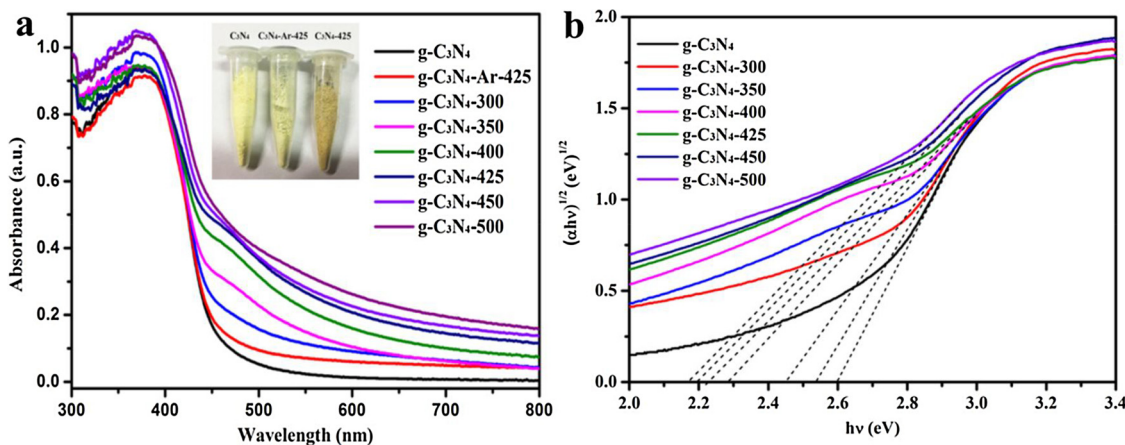


**Fig. 4.** (a) The UV–vis diffuse reflectance spectra of pristine g-C<sub>3</sub>N<sub>4</sub>, g-C<sub>3</sub>N<sub>4</sub> heated at 425 °C in Ar atmosphere alone and g-C<sub>3</sub>N<sub>4</sub> heated with NaH<sub>2</sub>PO<sub>2</sub> at different temperatures (300 °C, 350 °C, 400 °C, 425 °C, 450 °C and 500 °C) in Ar atmosphere, (b) the calculated band gaps for g-C<sub>3</sub>N<sub>4</sub> and g-C<sub>3</sub>N<sub>4</sub>-X (X means the temperature of heat treatment).

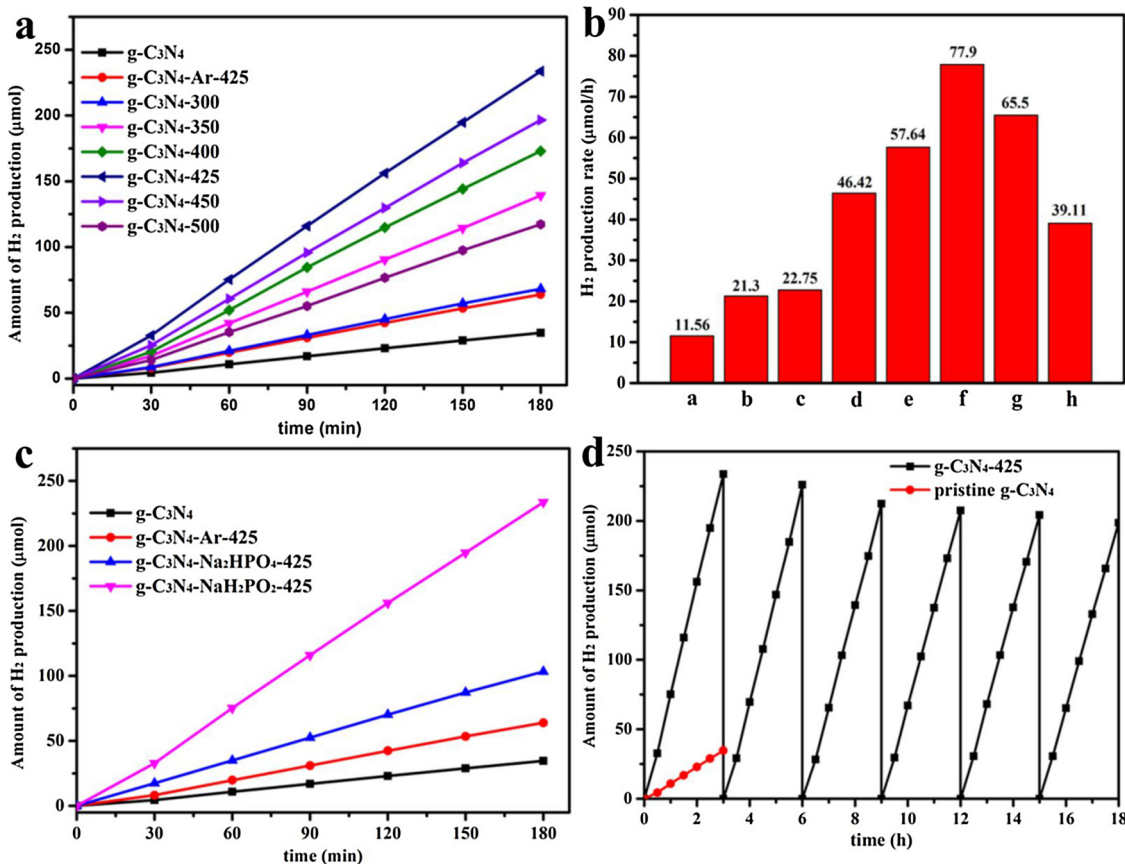


**Fig. 5.** (a) Time courses of H<sub>2</sub> production for pristine g-C<sub>3</sub>N<sub>4</sub>, g-C<sub>3</sub>N<sub>4</sub> heated without NaH<sub>2</sub>PO<sub>2</sub> at 425 °C in Ar atmosphere and g-C<sub>3</sub>N<sub>4</sub> heated with NaH<sub>2</sub>PO<sub>2</sub> at different temperatures in Ar atmosphere, (b) photocatalytic hydrogen production rates for the as-prepared products, a (pristine g-C<sub>3</sub>N<sub>4</sub>), b (g-C<sub>3</sub>N<sub>4</sub>-Ar-425), c (g-C<sub>3</sub>N<sub>4</sub>-300), d (g-C<sub>3</sub>N<sub>4</sub>-350), e (g-C<sub>3</sub>N<sub>4</sub>-400), f (g-C<sub>3</sub>N<sub>4</sub>-425), g (g-C<sub>3</sub>N<sub>4</sub>-450), h (g-C<sub>3</sub>N<sub>4</sub>-500), (c) comparison of photocatalytic H<sub>2</sub> production activities of pristine g-C<sub>3</sub>N<sub>4</sub>, g-C<sub>3</sub>N<sub>4</sub>-Ar-425, g-C<sub>3</sub>N<sub>4</sub>-Na<sub>2</sub>HPO<sub>4</sub>-425 and g-C<sub>3</sub>N<sub>4</sub>-NaH<sub>2</sub>PO<sub>4</sub>-425, (d) photocatalytic H<sub>2</sub> production curve of pristine g-C<sub>3</sub>N<sub>4</sub> and cyclic photocatalytic H<sub>2</sub> production curves for the g-C<sub>3</sub>N<sub>4</sub>-425 sample.

by H<sub>2</sub> production from water and CO<sub>2</sub> reduction. The photocatalytic H<sub>2</sub> production activities of all as-prepared products were evaluated under visible-light irradiation ( $\lambda \geq 420$  nm) using 1.0 wt % Pt as cocatalyst and triethanolamine as scavenger. Fig. 5a–b are a typical time course of hydrogen production and photocatalytic hydrogen production rates for pristine g-C<sub>3</sub>N<sub>4</sub>, g-C<sub>3</sub>N<sub>4</sub> heated without NaH<sub>2</sub>PO<sub>2</sub> at 425 °C in Ar atmosphere and g-C<sub>3</sub>N<sub>4</sub> heated with NaH<sub>2</sub>PO<sub>2</sub> at different temperatures in Ar atmosphere. Pristine g-C<sub>3</sub>N<sub>4</sub> shows a low photocatalytic H<sub>2</sub>

production rate (11.56 μmol/h), treating g-C<sub>3</sub>N<sub>4</sub> with NaH<sub>2</sub>PO<sub>2</sub> indeed enhances the activity. The hydrogen production rate gradually increases with the increased heating temperature from 300 °C to 425 °C. When the heating temperature rises to 425 °C, the highest hydrogen production rate is 77.9 μmol/h, which is nearly 6.7 times higher than that of pristine g-C<sub>3</sub>N<sub>4</sub>. In addition, the apparent quantum efficiency for H<sub>2</sub> production is 1.3% under 420 nm monochromatic irradiation. Further increasing the temperature, the photocatalytic performance

gradually weakens but still superior to the untreated g-C<sub>3</sub>N<sub>4</sub>, this could be attributed to the over-introduction of defects and structural damages. To further understand the reason for the increase in H<sub>2</sub> production, comparative test can be seen in Fig. 5c. G-C<sub>3</sub>N<sub>4</sub> heated at 425 °C in Ar atmosphere alone shows a little increase in H<sub>2</sub> production, which is consistent with previous reports [34]. The H<sub>2</sub> production activity of g-C<sub>3</sub>N<sub>4</sub> heated at 425 °C with Na<sub>2</sub>HPO<sub>4</sub> is higher than that of g-C<sub>3</sub>N<sub>4</sub> heated at 425 °C in Ar atmosphere alone, but still lower than that of g-C<sub>3</sub>N<sub>4</sub> heated at 425 °C with NaH<sub>2</sub>PO<sub>2</sub>. The cyano groups (—C≡N) is produced by the treatment of oxidizing Na<sub>2</sub>HPO<sub>4</sub>, the implantation of —C≡N groups as strong electron-withdrawing groups into the structure of g-C<sub>3</sub>N<sub>4</sub> can effectively promote the separation of the photo-generated carriers. P element doping can improve the light absorption, decrease the band gap energy and increase the electric conductivity [39]. Both the cyano groups (—C≡N) and P element are introduced into the g-C<sub>3</sub>N<sub>4</sub> system, which can further improve the H<sub>2</sub> production activity due to the synergistic effect. Stability is a very crucial criterion for practical application of photocatalyst, the photocatalytic stability of the optimized photocatalyst was evaluated by cycling experiments under prolonged visible light illumination duration of 18 h. As shown in Fig. 5d, the photocatalytic performance remains stable after six-round cycles, no obvious decrease in H<sub>2</sub> production rate is detected, indicating the high stability for photocatalytic H<sub>2</sub> production. In the process of practical application, AM1.5 is always adopted as light source in photocatalysis. The hydrogen production rate of g-C<sub>3</sub>N<sub>4</sub>-425 is 137.56 μmol/h under standard solar simulator (AM 1.5) irradiation, the detailed result can be seen in section 6, supporting information. Fig. 6a gives the action spectra (wavelength dependent) of H<sub>2</sub> production of 1.0 wt% Pt/g-C<sub>3</sub>N<sub>4</sub> under various monochromatic light irradiations (left axis). As can be seen, the variation tendency of H<sub>2</sub> production is similar to the UV/Vis light absorption spectrum (right axis). As we all know, g-C<sub>3</sub>N<sub>4</sub> obtained by urea precursor has superior performance than other precursor due to their large specific surface area. In order to further prove the universality of treatment method, we treated the g-C<sub>3</sub>N<sub>4</sub> obtained by urea precursor with the same method. The photocatalytic H<sub>2</sub> production tests are carried out under the same condition, Fig. 6b shows the comparison result of H<sub>2</sub> production. The hydrogen production rate of g-C<sub>3</sub>N<sub>4</sub> (precursor: urea) and g-C<sub>3</sub>N<sub>4</sub>-425 (precursor: urea) are 32 and 197.45 μmol/h, respectively. After heat treatment with NaH<sub>2</sub>PO<sub>2</sub>, the photocatalytic H<sub>2</sub> production performance gets improved about 6.17 times. In addition, the apparent quantum efficiency for H<sub>2</sub> production is 3.67% under 420 nm monochromatic irradiation. The detailed synthetic procedure, optical absorption properties and SEM images can be seen in section 10, supporting information.

In order to further verify the enhanced photocatalytic activity, photocatalytic CO<sub>2</sub> reduction was performed under visible-light irradiation ( $\lambda \geq 420$  nm) using 1.0 wt % Au as cocatalyst. No CO is found

without light irradiation or photocatalyst. From Fig. 7, CO is the main product and CH<sub>4</sub> is negligible in this experiment. No other by-products (e.g. CH<sub>3</sub>OH, formic acid, etc.) formed. It is difficult to accumulate multiple electrons to produce CH<sub>4</sub> molecule (eight electrons) and CH<sub>3</sub>OH molecule (six electrons), while only two electrons are needed for each CO molecule. And there are many reports that Au as cocatalyst exhibits good selectively for CO production during the photocatalytic CO<sub>2</sub> reduction. So the conversion of CO<sub>2</sub> to CO is a more dynamically favorable process during the photo-reduction. In order to confirm the source of CO, the contrast experiment was carried out without adding NaHCO<sub>3</sub> and bubbling high purity CO<sub>2</sub>, before irradiation, the system was vacuumized by vacuum pump and high purity Ar gas was bubbled for 30 min to ensure almost no CO<sub>2</sub> in the system. In Fig. 7a, only a little produced CO was detected from both pristine g-C<sub>3</sub>N<sub>4</sub> and g-C<sub>3</sub>N<sub>4</sub>-425 systems during the irradiation. The CO might come from tiny self-decomposition of g-C<sub>3</sub>N<sub>4</sub> during the irradiation. When NaHCO<sub>3</sub> and CO<sub>2</sub> were introduced into the systems, the CO yield increased a lot. The CO yield of pristine g-C<sub>3</sub>N<sub>4</sub> is 0.721 μmol/g, whereas the CO yield of g-C<sub>3</sub>N<sub>4</sub>-425 is 1.135 μmol/g after three hours' irradiation. Obviously, the photocatalytic activity of g-C<sub>3</sub>N<sub>4</sub>-425 is better than that of pristine g-C<sub>3</sub>N<sub>4</sub>. The stabilities of pristine g-C<sub>3</sub>N<sub>4</sub> and g-C<sub>3</sub>N<sub>4</sub>-425 were evaluated by cycling experiments. As shown in Fig. 7b, after the first three hours' irradiation, the CO yield decreases obviously, then, the performance decreases slowly in the next cycles. The drop in performance may result from tiny self-decomposition. The sample after cycles in CO<sub>2</sub> reduction was characterized by XPS, the peak intensity of P in the sample after cycles in CO<sub>2</sub> reduction reduced, the detailed results were shown in section 5, supporting information. But the photocatalytic activity of g-C<sub>3</sub>N<sub>4</sub>-425 is still better than that of pristine g-C<sub>3</sub>N<sub>4</sub> during the cycling experiment. Isotopic experiment was performed using <sup>13</sup>CO<sub>2</sub> (purity: 99%) to further prove the source of CO, and the produced CO was analyzed by gas chromatography-mass spectrometry (GC-MS). The detailed result can be seen in section 9, supporting information.

The morphology and microstructures of pristine g-C<sub>3</sub>N<sub>4</sub> and g-C<sub>3</sub>N<sub>4</sub>-425 are investigated by SEM and TEM. As shown in Fig. 8a and b, the SEM image of g-C<sub>3</sub>N<sub>4</sub>-425 exhibits the similar morphology with pristine g-C<sub>3</sub>N<sub>4</sub>, indicating that heated with NaH<sub>2</sub>PO<sub>2</sub> at 425 °C doesn't affect the main morphology and structure. In Fig. 8c and d, both pristine g-C<sub>3</sub>N<sub>4</sub> and g-C<sub>3</sub>N<sub>4</sub>-425 exhibit the typical two-dimensional structure consisting of multi-layer nanosheets. Importantly, it can be found that g-C<sub>3</sub>N<sub>4</sub>-425 possesses more pores in the layered structure as compared to pristine g-C<sub>3</sub>N<sub>4</sub>. The nano-porous structure is benefit for the photocatalytic activities. The BET surface areas of pristine g-C<sub>3</sub>N<sub>4</sub> and g-C<sub>3</sub>N<sub>4</sub>-425 were obtained by the nitrogen adsorption-desorption, the BET surface areas of g-C<sub>3</sub>N<sub>4</sub>-425 was 30.14 m<sup>2</sup>/g which was a little greater than pristine g-C<sub>3</sub>N<sub>4</sub> whose BET surface areas was 27.69 m<sup>2</sup>/g, the BET surface areas changed very little. So the enhancement of

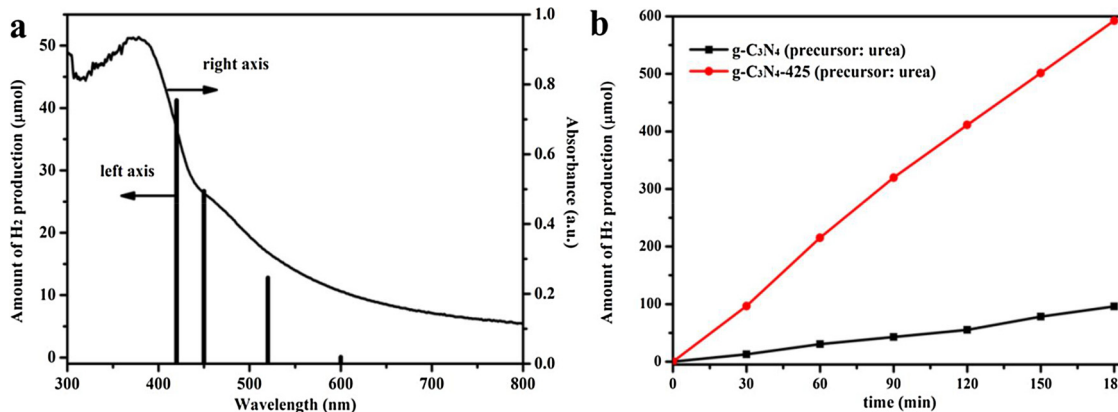
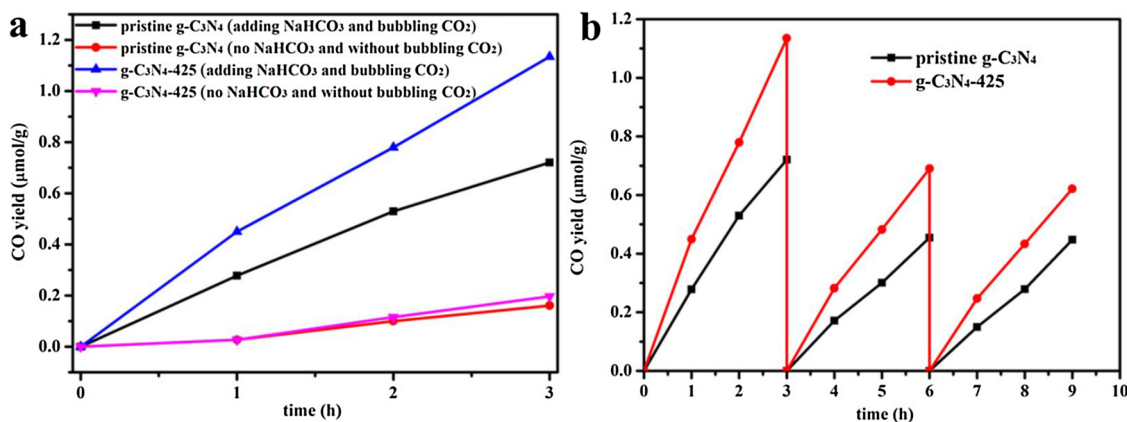


Fig. 6. (a) The action spectra (wavelength dependent) of H<sub>2</sub> production using 1.0 wt% Pt/g-C<sub>3</sub>N<sub>4</sub>-425 (left axis) and UV/Vis light absorption spectrum of g-C<sub>3</sub>N<sub>4</sub>-425 (right axis), (b) comparison of photocatalytic H<sub>2</sub> production activities of g-C<sub>3</sub>N<sub>4</sub> (precursor: urea) and g-C<sub>3</sub>N<sub>4</sub>-425 (precursor: urea).



**Fig. 7.** (a) Time courses of CO production for pristine g-C<sub>3</sub>N<sub>4</sub> and g-C<sub>3</sub>N<sub>4</sub>-425 with and without adding NaHCO<sub>3</sub> and bubbling high purity CO<sub>2</sub>, (b) cyclic photocatalytic CO production curves for the g-C<sub>3</sub>N<sub>4</sub>-425 and pristine g-C<sub>3</sub>N<sub>4</sub> samples.

photocatalytic H<sub>2</sub> production and CO<sub>2</sub> reduction are not just due to the weak increased BET surface areas. The STEM image of g-C<sub>3</sub>N<sub>4</sub>-425 and the corresponding EDS mappings of elemental C, N and P are shown in Fig. 9. In Fig. 9a, g-C<sub>3</sub>N<sub>4</sub>-425 exhibits the two-dimensional layer structure. The mixed EDS mappings of elemental C, N and P are shown in Fig. 9b, the red dots represent the elemental C, the green dots represent the elemental N and the blue dots represent the elemental P. The EDS mappings of C, N and P are presented in Fig. 9c–e, respectively. This result proves that P elemental presents in the g-C<sub>3</sub>N<sub>4</sub> system uniformly.

The effective generation and instant separation of photo-excited charge carriers are crucial for the photocatalytic reactions [44]. The room-temperature PL and TRPL (the time resolved fluorescence) spectra were measured to characterize the recombination rate and lifetime of photo-generated electrons and holes. As shown in Fig. 10a, the PL emission spectra of pristine g-C<sub>3</sub>N<sub>4</sub> and g-C<sub>3</sub>N<sub>4</sub>-425 exhibit a distinct peak at 455 nm caused by the recombination of photo-generated electrons and holes, which is consistent with variation of the band gap energy [10]. Obvious, the PL intensity of g-C<sub>3</sub>N<sub>4</sub>-425 is much lower

than that of pristine g-C<sub>3</sub>N<sub>4</sub>, and the decreased peak intensity further confirms a lower electron–hole recombination rate for g-C<sub>3</sub>N<sub>4</sub>-425 comparing with pristine g-C<sub>3</sub>N<sub>4</sub>. Moreover, the charge transfer dynamics for the two products are analyzed by the TRPL decay measurements (Fig. 10b), the average lifetime is calculated using the following relation:  $\tau_{av} = a_1\tau_1 + a_2\tau_2 + a_3\tau_3$ , ( $\tau_1, \tau_2$  and  $\tau_3$  are the lifetime,  $a_1, a_2$  and  $a_3$  are normalized pre-exponential factors) [3]. The average lifetime ( $\tau_{av}$ ) of g-C<sub>3</sub>N<sub>4</sub>-425 decreases to 3.96 ns, as compared to that of pristine g-C<sub>3</sub>N<sub>4</sub> (8.47 ns). These results imply that a new nonradiative decay pathway may be opened due to the charge transfer through the new channels and the photogenerated carriers of g-C<sub>3</sub>N<sub>4</sub>-425 are more quickly captured by reactive substrates and thus are able to drive redox reaction [40,45]. Photoelectrochemical measurements are used to further confirm the enhanced excitation and separation of the photo-generated carriers. Fig. 10c shows a comparison of the photocurrent-time curves for pristine g-C<sub>3</sub>N<sub>4</sub> and g-C<sub>3</sub>N<sub>4</sub>-425 with typical on-off cycles under visible light irradiation, the photocurrent response of g-C<sub>3</sub>N<sub>4</sub>-425 is higher than that of pristine g-C<sub>3</sub>N<sub>4</sub> strongly illustrating that the interface charge separation efficiency is improved. Meanwhile, to

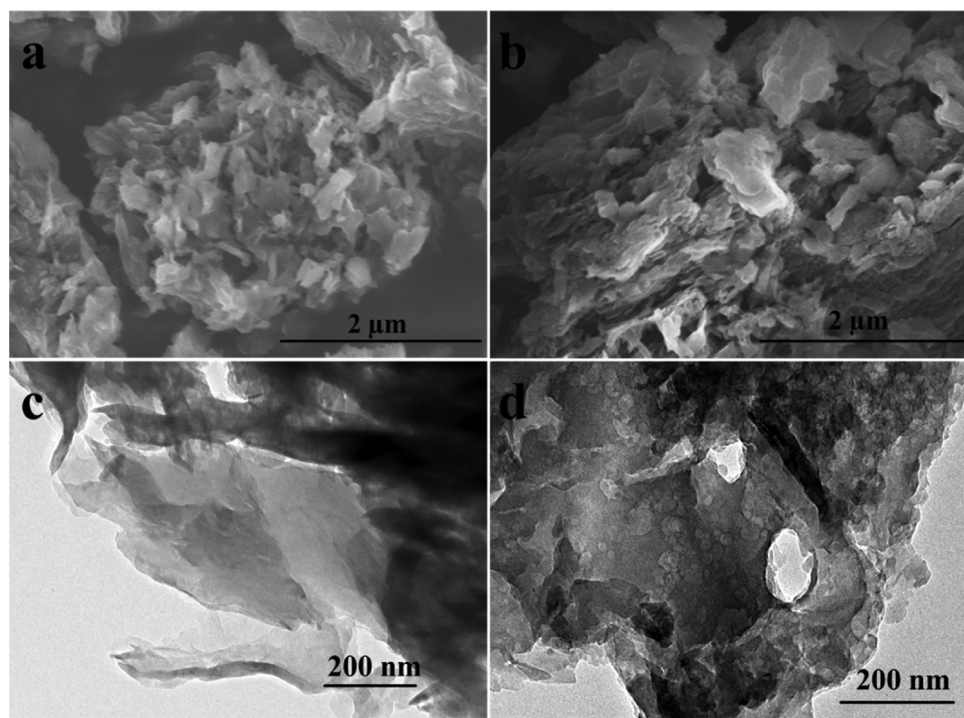


**Fig. 8.** SEM images of pristine g-C<sub>3</sub>N<sub>4</sub> (a) and g-C<sub>3</sub>N<sub>4</sub>-425 (b), TEM images of pristine g-C<sub>3</sub>N<sub>4</sub> (c) and g-C<sub>3</sub>N<sub>4</sub>-425 (d).

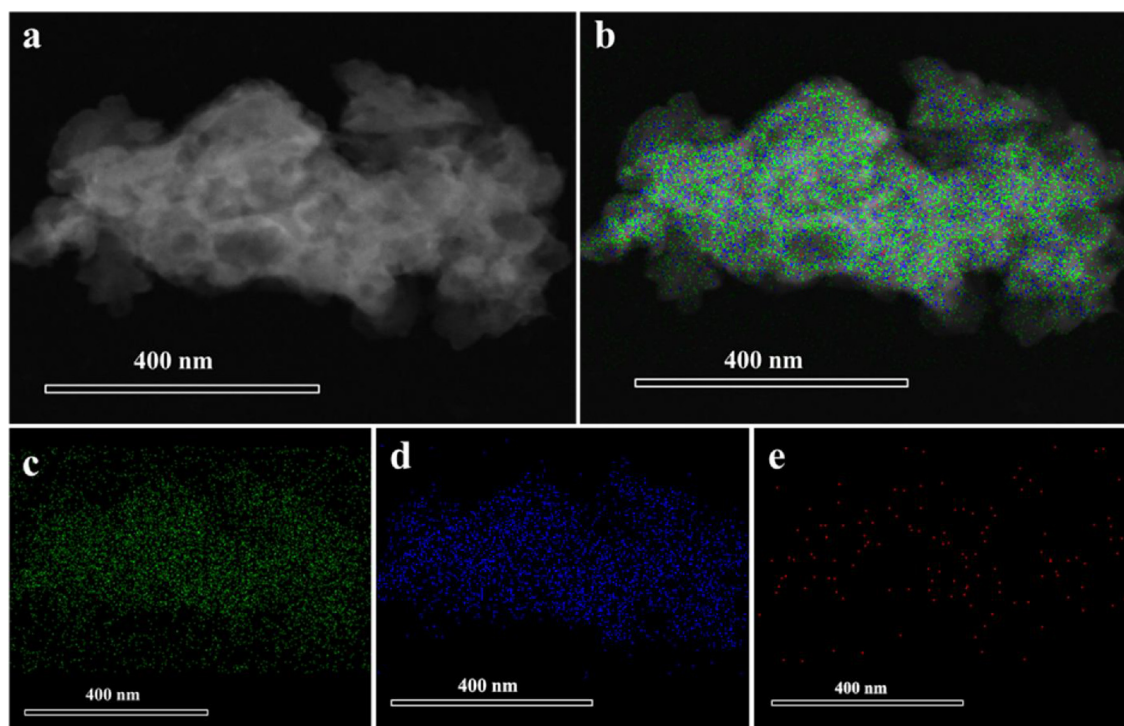


**Fig. 9.** (a) STEM images of g-C<sub>3</sub>N<sub>4</sub>-425, (b) mixed EDS mappings of elemental C, N and P in g-C<sub>3</sub>N<sub>4</sub>-425, (c–e) EDS mappings of elemental C (green dots), N (blue dots) and P (red dots), respectively (For interpretation of the references to colour in this figure legend, the reader is referred to the web version of this article).

gain deeper insight into the charge transport behavior of the both products in absence of light excitation, the electrochemical impedance spectroscopy (EIS) measurements were carried out under dark condition. An equivalent electronic circuit model (inset of Fig. 10d) was carried out to simulate the EIS test system, in which the R<sub>s</sub> and R<sub>ct</sub> stood for the total electrolyte solution resistance and the interfacial charge-transfer resistance, respectively. The diameters of the semicircular arc in the EIS Nyquist plots reflect the charge-transfer resistance of the working electrodes. In general, the smaller the diameter of semicircle arc of the EIS spectrum is, the lower the electron-transfer resistance value (R<sub>ct</sub>) is [46]. Compared with pristine g-C<sub>3</sub>N<sub>4</sub>, a smaller diameter of g-C<sub>3</sub>N<sub>4</sub>-425 is observed, indicating a good electronic conductivity in g-C<sub>3</sub>N<sub>4</sub>-425 sample. According to all of the results, the photo-excited charge carriers of g-C<sub>3</sub>N<sub>4</sub>-425 can be separated more effectively than that of pristine g-C<sub>3</sub>N<sub>4</sub>.

In order to investigate the band potentials (VB and CB) of pristine g-C<sub>3</sub>N<sub>4</sub> and g-C<sub>3</sub>N<sub>4</sub>-425, the VB XPS analysis was carried out, the detailed information can be seen in section 7, supporting information. In Fig. S7, the VB maximums of g-C<sub>3</sub>N<sub>4</sub> and g-C<sub>3</sub>N<sub>4</sub>-425 are 1.94 and 1.90 eV, respectively. The valence band potentials of g-C<sub>3</sub>N<sub>4</sub> and g-C<sub>3</sub>N<sub>4</sub>-425 are calculated to be 1.72 and 1.68 eV versus normal hydrogen electrode (NHE) at pH 7 using the formula E<sub>NHE</sub> = Φ + VBM - 4.5 (E<sub>NHE</sub> = the normal hydrogen electrode, Φ = 4.28 eV = the work function of the analyzer, namely, the Al metal). According to the formula E<sub>CB</sub> = E<sub>VB</sub> - E<sub>g</sub>, the CB minima of g-C<sub>3</sub>N<sub>4</sub> and g-C<sub>3</sub>N<sub>4</sub>-425 are determined to be -0.88 eV and -0.54 eV, respectively. Based on the above-discussed results, possible mechanism for enhanced photocatalytic H<sub>2</sub> production and CO<sub>2</sub> reduction activities has been discussed in Fig. 11. During the process of heating, NaH<sub>2</sub>PO<sub>2</sub> will decompose into gaseous PH<sub>3</sub> and solid-state Na<sub>2</sub>HPO<sub>4</sub> at temperature greater than 150 °C. According to the XPS and FTIR spectra analysis, the oxidizing solid-state Na<sub>2</sub>HPO<sub>4</sub> can react with terminal amino groups (-C-NH<sub>2</sub>) to produce cyano groups (-C≡N) and PH<sub>3</sub> can take part in P doping in g-C<sub>3</sub>N<sub>4</sub> system according to the formation of P-N bond. The reduced band gap energy of g-C<sub>3</sub>N<sub>4</sub>-425 can be seen from Fig. 11, so more visible light can be absorbed to produce more photogenerated carriers. The

photogenerated electrons can transfer to Pt or Au to take part in reduction reaction to produce H<sub>2</sub> or CO, the photogenerated holes can take part in oxidation reaction. As we all know, g-C<sub>3</sub>N<sub>4</sub> is a typical n-type material due to containing many terminal amino groups (-C-NH<sub>2</sub>) as electron donors, the produced cyano groups (-C≡N) as strong electron-withdrawing groups in g-C<sub>3</sub>N<sub>4</sub> system can promote the efficient separation of photo-generated electron-hole pairs, which can be proved by enhanced photocatalytic H<sub>2</sub> production in Fig. 5c. A simple heat treatment with NaH<sub>2</sub>PO<sub>2</sub> can bring so many advantages, more photo-excited charge carriers can be produced and separated to take part in the photocatalytic reactions, leading to higher efficiencies in photocatalytic H<sub>2</sub> production and CO<sub>2</sub> reduction.

#### 4. Conclusion

In summary, we developed a simple and effective method to prepare phosphorus and cyano groups (-C≡N) modified g-C<sub>3</sub>N<sub>4</sub> photocatalyst by NaH<sub>2</sub>PO<sub>2</sub> treatment at different temperatures in Ar atmosphere. After treatment, the intrinsic 2D layered structure was still maintained, the formation of cyano groups (-C≡N) can enhance the light absorption and act as strong electron-withdrawing groups, which can promote the efficient separation of photo-generated electron-hole pairs. Meanwhile, P element doping into the g-C<sub>3</sub>N<sub>4</sub> system enhances the visible light absorption, decreases the band gap energy, increases the electric conductivity and suppresses the recombination of photo-generated carriers. Together with these advantages, the photocatalytic H<sub>2</sub> production activity of the optimal g-C<sub>3</sub>N<sub>4</sub>-425 sample is nearly 6.7 times higher than that of pristine g-C<sub>3</sub>N<sub>4</sub> and 2.12 times higher than that of g-C<sub>3</sub>N<sub>4</sub> owning cyano groups alone, the photocatalytic CO<sub>2</sub> reduction activity of the optimal g-C<sub>3</sub>N<sub>4</sub>-425 sample is nearly 1.58 times higher than that of pristine g-C<sub>3</sub>N<sub>4</sub>. This work provides a simple and promising strategy to bring so many advantages to realize the highly effective photocatalytic activity.

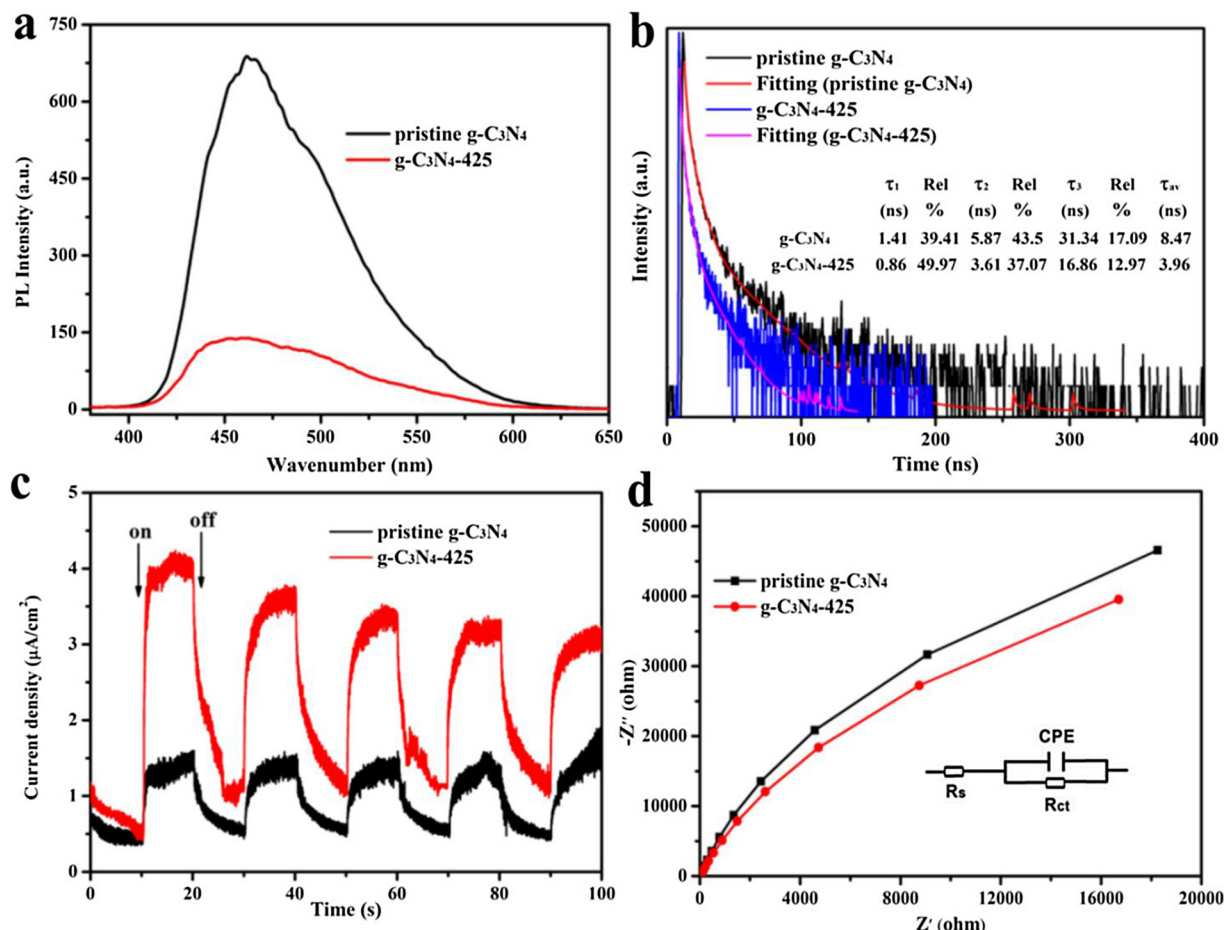


**Fig. 10.** (a) PL spectra of the pristine g-C<sub>3</sub>N<sub>4</sub> and g-C<sub>3</sub>N<sub>4</sub>-425 samples; (b) TRPL decay spectra of the pristine g-C<sub>3</sub>N<sub>4</sub> and g-C<sub>3</sub>N<sub>4</sub>-425 samples; (c) transient photocurrent responses of the pristine g-C<sub>3</sub>N<sub>4</sub> and g-C<sub>3</sub>N<sub>4</sub>-425 samples in 0.2 M Na<sub>2</sub>SO<sub>4</sub> aqueous solution with AM1.5 as light source; (d) EIS plots of the pristine g-C<sub>3</sub>N<sub>4</sub> and g-C<sub>3</sub>N<sub>4</sub>-425 samples in 0.2 M Na<sub>2</sub>SO<sub>4</sub> aqueous solution under standard solar simulator (AM 1.5) irradiation.

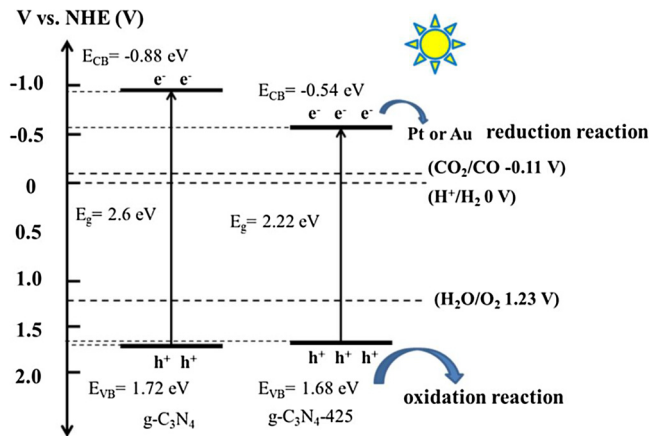


**Fig. 11.** Schematic illustration of the charge separation and transfer in g-C<sub>3</sub>N<sub>4</sub> and g-C<sub>3</sub>N<sub>4</sub>-425 system during the photocatalytic H<sub>2</sub> production and CO<sub>2</sub> reduction.

## Acknowledgements

This work was financially supported by a research grant from the National Natural Science Foundation of China (Nos. 51602179, 21333006, 21573135 and 11374190), and the National Basic Research Program of China (973 Program, No. 2013CB632401), Recruitment Program for Young Professionals, China and Taishan Scholar Foundation of Shandong Province, China.

## Appendix A. Supplementary data

Supplementary material related to this article can be found, in the online version, at doi:<https://doi.org/10.1016/j.apcatb.2018.03.094>.

## References

- [1] P.F. Xia, Z.B. Cheng, J.G. Yu, S.W. Cao, M. Jaroniec, *J. Mater. Chem. A* 5 (2017) 3230.
- [2] P.K. Chuang, K.H. Wu, T.F. Yeh, H. Teng, *ACS Sustainable Chem. Eng.* 4 (11) (2016) 5989–5997.
- [3] X.L. Liu, X.Z. Liang, P. Wang, B.B. Huang, X.Y. Qin, X.Y. Zhang, Y. Dai, *Appl. Catal. B: Environ.* 203 (2017) 282–288.
- [4] L.J. Liu, Y.Q. Jiang, H.L. Zhao, J.T. Chen, J.L. Cheng, K.S. Yang, Y. Li, *ACS Catal.* 6 (2) (2016) 1097–1108.
- [5] W.N. Xing, C.M. Li, G. Chen, Z.H. Han, Y.S. Zhou, Y.D. Hu, Q.Q. Meng, *Appl. Catal. B: Environ.* 203 (2017) 65–71.
- [6] F. Guo, J.L. Chen, M.W. Zhang, B.F. Gao, B.Z. Lin, Y.L. Chen, *J. Mater. Chem. A* 4 (2016) 10806.
- [7] J.D. Hong, X.Y. Xia, Y.S. Wang, R. Xu, *J. Mater. Chem.* 22 (2012) 15006–15012.
- [8] Q. Han, F. Zhao, C.G. Hu, L.X. Lv, Z.P. Zhang, N. Chen, L.T. Qu, *Nano Res.* 8 (5) (2015) 1718.
- [9] M.L. Li, L.X. Zhang, X.Q. Fan, M.Y. Wu, M. Wang, R.L. Cheng, L.L. Zhang, H.L. Yao, J.L. Shi, *Appl. Catal. B: Environ.* 201 (2017) 629–635.
- [10] K. Wang, Q. Li, B.S. Liu, B. Cheng, W.K. Ho, J.G. Yu, *Appl. Catal. B: Environ.* 176 (2015) 44–52.
- [11] W.J. Ong, L.K. Putri, Y.C. Tan, L.L. Tan, N. Li, Y.H. Ng, X.M. Wen, S.P. Chai, *Nano Res.* 10 (5) (2017) 1673–1696.
- [12] S. Cao, J. Low, J. Yu, M. Jaroniec, *Adv. Mater.* 27 (13) (2015) 2150–2176.
- [13] D.D. Zheng, C.Y. Pang, Y.X. Liu, X.C. Wang, *Chem. Commun.* 51 (2015) 9706.
- [14] J. Xu, Y.J. Wang, Y.F. Zhu, *Langmuir* 29 (2013) 10566–10572.
- [15] H.J. Yan, *Chem. Commun.* 48 (2012) 3430–3432.
- [16] H.W. Huang, K. Xiao, N. Tian, F. Dong, T.R. Zhang, X. Du, Y.H. Zhang, *J. Mater. Chem. A* 5 (2017) 17452–17463.

- [17] C.Y. Liu, Y.H. Zhang, F. Dong, X. Du, H.W. Huang, *J. Phys. Chem. C* 120 (19) (2016) 10381–10389.
- [18] B.H. Long, Y. Zheng, L.H. Lin, K.A. Alamry, A.M. Asiri, X.C. Wang, *J. Mater. Chem. A* 5 (2017) 16179–16188.
- [19] G. Liu, P. Niu, C.H. Sun, S.C. Smith, Z.G. Chen, G.Q. Lu, H.M. Cheng, *J. Am. Chem. Soc.* 132 (2010) 11642.
- [20] W. Chen, T.Y. Liu, T. Huang, X.H. Liu, X.J. Yang, *Nanoscale* 8 (2016) 3711.
- [21] J.R. Ran, T.Y. Ma, G.P. Gao, X.W. Du, S.Z. Qiao, *Energy Environ. Sci.* 8 (2015) 3708.
- [22] X.J. She, H. Xu, Y.G. Xu, J. Yan, J.X. Xia, L. Xu, Y.H. Song, Y. Jiang, Q. Zhang, H.M. Li, *J. Mater. Chem. A* 2 (2014) 2563.
- [23] C.C. Feng, Z.H. Wang, Y. Ma, Y.J. Zhang, L. Wang, Y.P. Bi, *Appl. Catal. B: Environ.* 205 (2017) 19–23.
- [24] W.J. Wang, H.F. Cheng, B.B. Huang, X.L. Liu, X.Y. Qin, X.Y. Zhang, Y. Dai, *J. Colloid Interface Sci.* 442 (2015) 97–102.
- [25] C.S. Pan, J. Xu, Y.J. Wang, D. Li, Y.F. Zhu, *Adv. Funct. Mater.* 22 (7) (2012) 1518–1524.
- [26] N. Tian, H.W. Huang, C.Y. Liu, F. Dong, T.R. Zhang, X. Du, S.X. Yu, Y.H. Zhang, *J. Mater. Chem. A* 3 (2015) 17120–17129.
- [27] C.C. Han, L.E. Wu, L. Ge, Y.J. Li, Z. Zhao, *Carbon* 92 (2015) 31–40.
- [28] Z.H. Chen, P. Sun, B. Fan, Z.G. Zhang, X.M. Fang, *J. Phys. Chem. C* 118 (2014) 7801–7807.
- [29] D.Q. Zeng, W.J. Ong, H.F. Zheng, M.D. Wu, Y.Z. Chen, D.L. Peng, M.Y. Han, *J. Mater. Chem. A* 5 (31) (2017) 16171–16178.
- [30] Z.M. Pan, Y. Zheng, F.S. Guo, P.P. Niu, X.C. Wang, *ChemSusChem* 10 (2017) 87–90.
- [31] D.Q. Zeng, W.J. Xu, W.J. Ong, J. Xu, H. Ren, Y.Z. Chen, H.F. Zheng, D.L. Peng, *Appl. Catal. B: Environ.* (2017), <http://dx.doi.org/10.1016/j.apcatb.2017.08.041>.
- [32] G.G. Zhang, Z.A. Lan, X.C. Wang, *Chem. Sci.* 8 (2017) 5261–5274.
- [33] G.G. Liu, G.X. Zhao, W. Zhou, Y.Y. Liu, H. Pang, H.B. Zhang, D. Hao, X.G. Meng, P. Li, T. Kako, J.H. Ye, *Adv. Funct. Mater.* 26 (37) (2016) 6822–6829.
- [34] Y.Y. Kai, Y.Q. Yang, L.C. Yin, X.D. Kang, G. Liu, H.M. Cheng, *Adv. Mater.* 27 (31) (2015) 4572–4577.
- [35] P. Niu, L.C. Yin, Y.Q. Yang, G. Liu, H.M. Cheng, *Adv. Mater.* 26 (2014) 8046.
- [36] L.Q. Yang, J.F. Huang, L. Shi, L.Y. Cao, Q. Yu, Y.N. Jie, J. Fei, H.B. Ouyang, J.H. Ye, *Appl. Catal. B: Environ.* 204 (2017) 335–345.
- [37] Q.L. Tay, P. Kanhere, C.F. Ng, S. Chen, S. Chakraborty, A.C.H. Huan, T.C. Sum, R. Ahuja, Z. Chen, *Chem. Mater.* 27 (2015) 4930–4933.
- [38] T. Zhai, L.M. Wan, S. Sun, Q. Chen, J. Sun, Q.Y. Xia, H. Xia, *Adv. Mater.* 29 (2017) 1604167.
- [39] S.E. Guo, Z.P. Deng, M.X. Li, B.J. Jiang, C.G. Tian, Q.J. Pan, H.G. Fu, *Angew. Chem. Int. Ed.* 55 (5) (2016) 1830–1834.
- [40] S.W. Cao, Q. Huang, B.C. Zhu, J.G. Yu, *J. Power Sources* 351 (2017) 151–159.
- [41] X. Wang, K. Maeda, A. Thomas, K. Takanabe, G. Xin, J.M. Carlsson, K. Domen, M. Antonietti, *Nat. Mater.* 8 (2009) 76–80.
- [42] H.J. Yu, R. Shi, Y.X. Zhao, T. Bian, Y.F. Zhao, C. Zhou, G.I.N. Waterhouse, L.Z. Wu, C.H. Tung, T.R. Zhang, *Adv. Mater.* (16) (2017) 29.
- [43] H.L. Gao, S.C. Yan, J.J. Wang, Y.A. Huang, P. Wang, Z.S. Li, Z.G. Zou, *Phys. Chem. Chem. Phys.* 15 (2013) 18077.
- [44] X.L. Liu, W.J. Wang, Y.Y. Liu, B.B. Huang, Y. Dai, X.Y. Qin, X.Y. Zhang, *RSC Adv.* 5 (69) (2015) 55957–55963.
- [45] N. Tian, Y.H. Zhang, X.W. Li, K. Xiao, X. Du, F. Dong, G.I.N. Waterhouse, T.R. Zhang, H.W. Huang, *Nano Energy* 38 (2017) 72–81.
- [46] Y.P. Zhu, T.Z. Ren, Z.Y. Yuan, *ACS Appl. Mater. Interfaces* 7 (30) (2015) 16850–16856.